Investigation of Numerical Errors of the Two-Dimensional ADI–FDTD Method

Takefumi Namiki, *Member, IEEE,* and Koichi Ito, *Member, IEEE*

***Abstract*—We previously proposed the ADI–FDTD method as a means of solving two-dimensional Maxwell's equations. The algorithm used in this method is unconditionally stable, which means the time-step size can be set arbitrarily when this method is used. The limitation of the time-step size is not dependent on the Courant–Friedrich–Levy (CFL) condition, but on numerical errors such as numerical dispersion. In this paper, we investigate the numerical errors of the method quantitatively and discuss the calculation accuracy and efficiency of the method. We found that a large time-step size results in high numerical dispersion. However, the limit of the time-step size due to numerical dispersion is greater than the CFL limit if the size of the local minimum cell in the computational domain is much smaller than the other cells and the wavelength. In that case, because the large time-step size reduces the number of time-loop iterations, the ADI–FDTD method is more efficient than the conventional FDTD method in terms of computer resources such as central processing unit time.**

***Index Terms*—ADI–FDTD method, CFL condition, FDTD method, numerical dispersion.**

I. Introduction

WE PREVIOUSLY proposed the alternating direction implicit (ADI)–finite-difference time-domain (FDTD) method as a means of solving the two-dimensional (2-D) TE wave [1]. This method is based on the ADI method [2] and is applied to Yee's staggered cell [3] to solve Maxwell's equations. The algorithm is unconditionally stable, which means the time-step size can be set arbitrarily when this method is used. The limitation of the maximum time-step size of this method is not dependent on the Courant–Friedrich–Levy (CFL) condition, but rather on numerical errors.

In this paper, we undertook a quantitative study on the selection of the time-step size in the ADI–FDTD method for 2-D TM and TE waves in terms of numerical error. We demonstrated the 2-D ADI–FDTD method using various time-step sizes and compared the results with that of the conventional FDTD method from the viewpoint of accuracy and efficiency.

Section II provides numerical formulations of the ADI–FDTD method for 2-D TM and TE waves. In Section III, the methods used to estimate numerical error, such as numerical dispersion and amplitude error, are explained. Section IV provides the numerical results of error estimations. In Section V, we discuss the selection of time-step size in the ADI–FDTD method in terms of numerical error.

Manuscript received August 5, 1999.

T. Namiki is with the Computational Science and Engineering Center, Fujitsu Limited, Chiba 261-8588, Japan (e-mail: namiki@strad.se.fujitsu.co.jp).

K. Ito is with the Faculty of Engineering, Chiba University, Chiba 263-8522, Japan (e-mail: ito@cute.te.chiba-u.ac.jp).

Publisher Item Identifier S 0018-9480(00)09547-8.

II. Numerical Formulations of the 2-D ADI–FDTD Method

A. For a 2D TM Wave

The numerical formulation of the ADI–FDTD method for a 2D TM wave is presented in (1)–(6). The electromagnetic-field components are arranged on the cells in the same way as that when the conventional FDTD method is used. These formulations are available for an inhomogeneous lossy medium and when nonuniform cells are used. Two procedures are used to calculate one discrete time-step. The first procedure is based on (1)–(3), and the second procedure is based on (4)–(6) as follows:

⟨First procedure⟩

$$H_x^{n+1/2}(i, j+1/2) = H_x^n(i, j+1/2) - B_b(i, j+1/2) \cdot \left\{E_z^n(i, j+1) - E_z^n(i, j)\right\} \tag{1}$$

$$H_y^{n+1/2}(i+1/2, j) = H_y^n(i+1/2, j) + B_a(i+1/2, j) \cdot \left\{E_z^{n+1/2}(i+1, j) - E_z^{n+1/2}(i, j)\right\} \tag{2}$$

$$E_z^{n+1/2}(i, j) = C(i, j) \cdot E_z^n(i, j) + D_a^n(i, j) \cdot \left\{H_y^{n+1/2}(i+1/2, j) - H_y^{n+1/2}(i-1/2, j)\right\} - D_b^n(i, j) \cdot \left\{H_x^n(i, j+1/2) - H_x^n(i, j-1/2)\right\} \tag{3}$$

⟨Second procedure⟩

$$H_x^{n+1}(i, j+1/2) = H_x^{n+1/2}(i, j+1/2) - B_b(i, j+1/2) \cdot \left\{E_z^{n+1}(i, j+1) - E_z^{n+1}(i, j)\right\} \tag{4}$$

$$H_y^{n+1}(i+1/2, j) = H_y^{n+1/2}(i+1/2, j) + B_a(i+1/2, j) \cdot \left\{E_z^{n+1/2}(i+1, j) - E_z^{n+1/2}(i, j)\right\} \tag{5}$$

$$E_z^{n+1}(i, j) = C(i, j) \cdot E_z^{n+1/2}(i, j) + D_a^n(i, j) \cdot \left\{H_y^{n+1/2}(i+1/2, j) - H_y^{n+1/2}(i-1/2, j)\right\} - D_b^n(i, j) \cdot \left\{H_x^{n+1}(i, j+1/2) - H_x^{n+1}(i, j-1/2)\right\} \tag{6}$$

where the coefficients are defined in the same way as in the conventional FDTD method as follows:

$$B_a(i,j)=\frac{\Delta t}{\mu(i,j)}\cdot\frac{1}{\Delta x(i)}$$
$$B_b(i,j)=\frac{\Delta t}{\mu(i,j)}\cdot\frac{1}{\Delta y(j)}$$
$$C(i,j)=\frac{\varepsilon(i,j)}{\varepsilon(i,j)+\sigma(i,j)\Delta t}$$
$$D_a(i,j)=\frac{\Delta t}{\varepsilon(i,j)+\sigma(i,j)\Delta t}\cdot\frac{1}{\Delta x(i)}$$
$$D_b(i,j)=\frac{\Delta t}{\varepsilon(i,j)+\sigma(i,j)\Delta t}\cdot\frac{1}{\Delta y(j)}.$$

In the first procedure, (2) and (3) cannot be used for direct numerical calculation, thus, (3') is derived from (2) and (3) by eliminating the $H_y^{n+1/2}$ components. In the suffix "i," (3') indicates i maximum number of simultaneous linear equations. Thereafter, (2) can be used to calculate directly using the $E_z^{n+1/2}$ components calculated with (3') as follows:

$$\begin{aligned}&\alpha E_z^{n+1/2}(i-1,j)+\beta E_z^{n+1/2}(i,j)+\gamma E_z^{n+1/2}(i+1,j)\\&\quad=C(i,j)\cdot E_z^n(i,j)+D_a(i,j)\\&\qquad\cdot\left\{H_y^n(i+1/2,j)-H_y^n(i-1/2,j)\right\}\\&\qquad-D_b(i,j)\cdot\left\{H_x^n(i,j+1/2)-H_x^n(i,j+1/2)\right\}\end{aligned}\tag{3'}$$

where

$$\alpha=-B_a(i-1/2,j)\cdot D_a(i,j)$$
$$\gamma=-B_a(i+1/2,j)\cdot D_a(i,j)$$
$$\beta=1-\alpha-\gamma.$$

In the second procedure, (4) and (6) also cannot be used for direct numerical calculation, thus, (6') is derived from (4) and (6) by eliminating the H_x^{n+1} components. In the suffix "j," (6') indicates j maximum number of simultaneous linear equations. Thereafter, (4) can be used to calculate directly using the E_z^{n+1} components calculated by (6') as follows:

$$\begin{aligned}&\alpha E_z^{n+1}(i,j-1)+\beta E_z^{n+1}(i,j)+\gamma E_z^{n+1}(i,j+1)\\&\quad=C(i,j)\cdot E_z^{n+1/2}(i,j)+D_a(i,j)\\&\qquad\cdot\left\{H_y^{n+1/2}(i+1/2,j)-H_y^{n+1/2}(i-1/2,j)\right\}-D_b(i,j)\\&\qquad\cdot\left\{H_x^{n+1/2}(i,j+1/2)-H_x^{n+1/2}(i,j+1/2)\right\}\end{aligned}\tag{6'}$$

where

$$\alpha=-B_b(i,j-1/2)\cdot D_b(i,j)$$
$$\gamma=-B_b(i,j+1/2)\cdot D_b(i,j)$$
$$\beta=1-\alpha-\gamma.$$

Since simultaneous linear equations (3') and (6') can be written in tridiagonal matrix form, the computational costs are not very high.

B. For a 2D TE Wave

The numerical formulation of the ADI–FDTD method for a 2D TE wave is presented in (7)–(12). The calculation is made in the same way as in the case of the TM wave as follows:

⟨**First procedure**⟩

$$\begin{aligned}&E_x^{n+1/2}(i+1/2,j)\\&\quad=C(i+1/2,j)\cdot E_x^n(i+1/2,j)+D_b(i+1/2,j)\\&\qquad\cdot\left\{H_z^n(i+1/2,j+1/2)-H_z^n(i+1/2,j-1/2)\right\}\end{aligned}\tag{7}$$

$$\begin{aligned}&E_y^{n+1/2}(i,j+1/2)\\&\quad=C(i,j+1/2)\cdot E_y^n(i,j+1/2)-D_a(i,j+1/2)\\&\qquad\cdot\left\{H_z^{n+1/2}(i+1/2,j+1/2)-H_z^{n+1/2}(i-1/2,j+1/2)\right\}\end{aligned}\tag{8}$$

$$\begin{aligned}&H_z^{n+1/2}(i+1/2,j+1/2)\\&\quad=H_z^n(i+1/2,j+1/2)+B_b(i+1/2,j+1/2)\\&\qquad\cdot\left\{E_x^n(i+1/2,j+1)-E_x^n(i+1/2,j)\right\}\\&\qquad-B_a(i+1/2,j+1/2)\\&\qquad\cdot\left\{E_y^{n+1/2}(i+1,j+1/2)-E_y^{n+1/2}(i,j+1/2)\right\}\end{aligned}\tag{9}$$

⟨**Second procedure**⟩

$$\begin{aligned}&E_x^{n+1}(i+1/2,j)\\&\quad=C(i+1/2,j)\cdot E_x^{n+1/2}(i+1/2,j)+D_b(i+1/2,j)\\&\qquad\cdot\left\{H_z^{n+1}(i+1/2,j+1/2)-H_z^{n+1}(i+1/2,j-1/2)\right\}\end{aligned}\tag{10}$$

$$\begin{aligned}&E_y^{n+1}(i,j+1/2)\\&\quad=C(i,j+1/2)\cdot E_y^{n+1/2}(i,j+1/2)-D_a(i,j+1/2)\\&\qquad\cdot\left\{H_z^{n+1/2}(i+1/2,j+1/2)-H_z^{n+1/2}(i-1/2,j+1/2)\right\}\end{aligned}\tag{11}$$

$$\begin{aligned}&H_z^{n+1}(i+1/2,j+1/2)\\&\quad=H_z^{n+1/2}(i+1/2,j+1/2)+B_b(i+1/2,j+1/2)\\&\qquad\cdot\left\{E_x^{n+1}(i+1/2,j+1)-E_x^{n+1}(i+1/2,j)\right\}\\&\qquad-B_a(i+1/2,j+1/2)\\&\qquad\cdot\left\{E_y^{n+1/2}(i+1,j+1/2)-E_y^{n+1/2}(i,j+1/2)\right\}.\end{aligned}\tag{12}$$

In the first procedure, (8) and (9) cannot be used for direct numerical calculation, thus, (8') is derived from (8) and (9) by eliminating the $H_z^{n+1/2}$ components as follows:

$$\begin{aligned}&\alpha E_y^{n+1/2}(i-1,j+1/2)+\beta E_y^{n+1/2}(i,j+1/2)\\&\qquad+\gamma E_y^{n+1/2}(i+1,j+1/2)\\&\quad=C(i,j+1/2)\cdot E_y^n(i,j+1/2)+D_a(i,j+1/2)\\&\qquad\cdot\Big[\left\{H_z^n(i-1/2,j+1/2)-H_z^n(i+1/2,j+1/2)\right\}\\&\qquad\quad-B_b(i+1/2,j+1/2)\\&\qquad\quad\cdot\left\{E_x^n(i+1/2,j+1)-E_x^n(i+1/2,j)\right\}\\&\qquad\quad+B_b(i-1/2,j+1/2)\\&\qquad\quad\cdot\left\{E_x^n(i-1/2,j+1)-E_x^n(i-1/2,j)\right\}\Big]\end{aligned}\tag{8'}$$

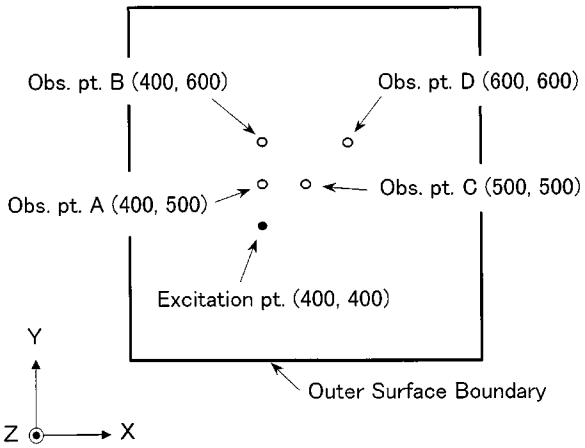

Fig. 1. Free-space model for a 2-D TM wave.

where

$$\alpha = -B_a(i-1/2,\, j+1/2)\cdot D_a(i,\, j+1/2)$$
$$\gamma = -B_a(i+1/2,\, j+1/2)\cdot D_a(i,\, j+1/2)$$
$$\beta = 1-\alpha-\gamma.$$

In the second procedure, (10) and (12) cannot be used for direct numerical calculation, thus, (10') is derived from (10) and (12) by eliminating the $H_z^{n+1/2}$ components as follows:

$$\begin{aligned}
&\alpha E_x^{n+1}(i+1/2,\, j-1)+\beta E_x^{n+1}(i+1/2,\, j)\\
&\quad +\gamma E_x^{n+1}(i+1/2,\, j+1)\\
&\quad = C(i+1/2,\, j)\cdot E_x^{n+1/2}(i+1/2,\, j)+D_b(i+1/2,\, j)\\
&\qquad \cdot\Big[\big\{H_z^{n+1/2}(i+1/2,\, j+1/2)\\
&\qquad\quad -H_z^{n+1/2}(i+1/2,\, j-1/2)\big\}\\
&\qquad\quad -B_a(i+1/2,\, j+1/2)\\
&\qquad\quad \cdot\big\{E_y^{n+1/2}(i+1,\, j+1/2)-E_y^{n+1/2}(i,\, j+1/2)\big\}\\
&\qquad\quad +B_a(i+1/2,\, j-1/2)\\
&\qquad\quad \cdot\big\{E_y^{n+1/2}(i+1,\, j-1/2)-E_y^{n+1/2}(i,\, j-1/2)\big\}\Big]
\end{aligned} \tag{10'}$$

where

$$\alpha = -B_b(i+1/2,\, j-1/2)\cdot D_b(i+1/2,\, j)$$
$$\gamma = -B_b(i+1/2,\, j+1/2)\cdot D_b(i+1/2,\, j)$$
$$\beta = 1-\alpha-\gamma.$$

III. Numerical Simulations for Error Estimation

In order to investigate the relationship between the time-step size and numerical error of the ADI–FDTD method, we performed numerical simulations using several models. For a 2-D TM wave, the free-space model shown in Fig. 1 was used. For a 2-D TE wave, the parallel-plate waveguide model, shown in Fig. 2, was used. We also used uniform and nonuniform cells for both models. The cell sizes were as follows:

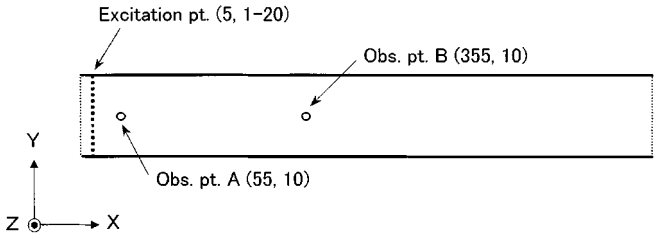

Fig. 2. Parallel-plate waveguide model for a 2-D TE wave.

⟨*Model 1-a*⟩: A free-space model for a TM wave using uniform cells was as follows:

$$dx(i) = \Delta(1 \le i \le 1000) \quad dy(j) = \Delta(1 \le j \le 1000).$$

The CFL condition of this model was as follows:

$$\Delta t \le \frac{\Delta}{c\sqrt{2}}.$$

⟨*Model 1-b*⟩: A free-space model for a TM wave using local nonuniform cells was as follows:

$$dx(i) = \begin{cases} \Delta, & 1 \le i \le 546,\ 555 \le i \le 1000\\ \Delta/2, & i = 547,\ 554\\ \Delta/2^2, & i = 548,\ 553\\ \Delta/2^3, & i = 549,\ 552\\ \Delta/2^4, & i = 550,\ 551 \end{cases}$$
$$dy(j) = \begin{cases} \Delta, & 1 \le j \le 546,\ 555 \le j \le 1000\\ \Delta/2, & j = 547,\ 554\\ \Delta/2^2, & j = 548,\ 553\\ \Delta/2^3, & j = 549,\ 552\\ \Delta/2^4, & j = 550,\ 551. \end{cases}$$

The CFL condition of this model was as follows:

$$\Delta t \le \frac{\Delta}{c\sqrt{2^9}}.$$

⟨*Model 2-a*⟩: A parallel-plate waveguide model for a TE wave using uniform cells was as follows:

$$dx(i) = \Delta(1 \le i \le 1000) \quad dy(j) = \Delta(1 \le j \le 20).$$

The CFL condition of this model was as follows:

$$\Delta t \le \frac{\Delta}{c\sqrt{2}}.$$

⟨*Model 2-b*⟩: A parallel-plate waveguide model for a TE wave using local nonuniform cells was as follows:

$$dx(i) = \begin{cases} \Delta, & 1 \le i \le 201,\ 210 \le i \le 1000\\ \Delta/2, & i = 202,\ 209\\ \Delta/2^2, & i = 203,\ 208\\ \Delta/2^3, & i = 204,\ 207\\ \Delta/2^4, & i = 205,\ 206 \end{cases}$$
$$dy(j) = \Delta(1 \le j \le 20).$$

The CFL condition of this model was as follows:

$$\Delta t \le \frac{\Delta}{c\sqrt{2^8+1}}.$$

Since every model was prepared with sufficient number of cells to separate the reflection waves occurring at the outer sur-

face boundaries from the propagation wave in the time domain, it was not necessary to consider the accuracy of the absorbing boundary condition during this investigation.

The excitation was applied at the electric-field components (E_z or E_y) at the excitation points, and the electric-field components of the observation points were then output. The waveform of the excitation pulse was as follows:

$$E = E - E_0(t - t_0)\exp\left[-\frac{(t-t_0)^2}{T^2}\right]$$

where

$$t_0 = 186\Delta t_0 \quad T = 50\Delta t_0 \quad \Delta t_0 = \Delta \Big/ \left(c\sqrt{2}\right).$$

The numerical dispersion was estimated as follows [4]. The Fourier transforms of $E(t)$ at two different points were given by

$$E(\omega, r_1) = \int_{-\infty}^{\infty} E(t, r_1)\cdot e^{-j\omega t}\,dt \tag{13a}$$

$$E(\omega, r_2) = \int_{-\infty}^{\infty} E(t, r_2)\cdot e^{-j\omega t}\,dt \tag{13b}$$

where (r_1, r_2) indicated point (A, B) or point (C, D).

Taking the ratio, we could obtain the propagation constants α and β of the wave as follows:

$$e^{-[\alpha(\omega)+j\beta(\omega)]L} = \frac{E(\omega, r_2)}{E(\omega, r_1)}$$

where L was the distance between r_1 and r_2.

The phase velocity v_p was given by

$$v_p(\omega) = \frac{\omega}{\beta(\omega)}.$$

We estimated numerical dispersion with the phase velocity normalized by the speed of light c.

The numerical amplitude error was calculated as follows. We could obtain the amplitude of the electric field at point r_2 directly from (13b). On the other hand, in the Fig. 1 model, since the propagation wave was a cylindrical wave, the amplitude of E_z at point r_2 should be equal to the amplitude given by $|E_z(\omega, r_1)|\cdot\sqrt{L_1}/\sqrt{L_2}$, where L_1, L_2 indicated the distances from the excitation point to r_1, r_2, respectively. In the Fig. 2 model, the amplitude of E_y at point r_2 should be equal to that at point r_1. We estimated the numerical amplitude error using the value of $|E_y(\omega, r_2)|$ normalized by the amplitude calculated using $|E_y(\omega, r_1)|$.

We performed these numerical simulations using the ADI–FDTD method and various time-step sizes.

IV. Numerical Results

⟨*Model 1-a*⟩*:* Figs. 3 and 4 show the normalized phase velocity versus frequency, which was normalized by the value of $c/(100\Delta)$. These figures include the results of several simulations performed with different time-step sizes, which was normalized by Δt_0. The data of Fig. 3, which was derived from data observed at points A and B, indicates that the propagation angle of the wave was 90°. The data of Fig. 4, which was derived from data observed at points C and D, indicates that the propagation angle was 45°.

In both cases, an increase in the time-step size resulted in a decrease in phase velocity. If the propagation angles were identical, the decrease was substantial at a higher frequency. If the frequency was the same, the decrease was substantial for a 90°-angle propagation.

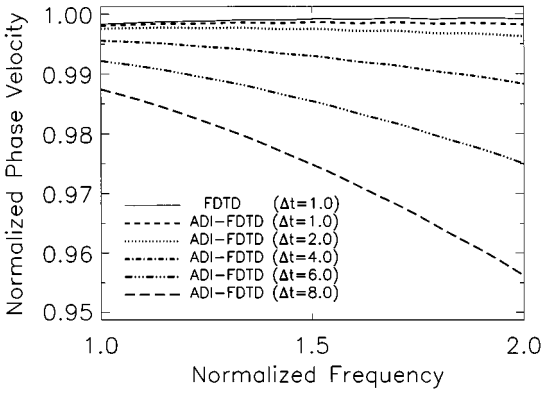

Fig. 3. Normalized phase velocity versus normalized frequency of model 1-a. The propagation angle was 90° (propagated along the y-axis). This figure included the results performed with different time-step sizes.

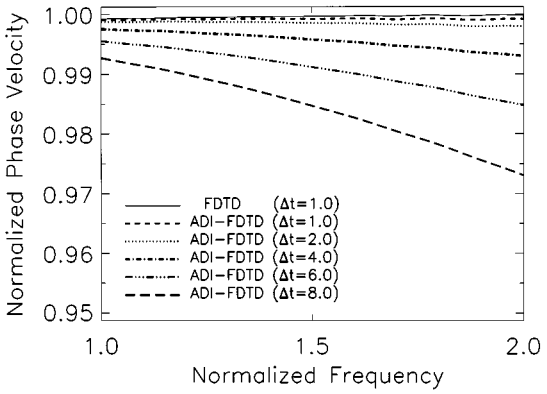

Fig. 4. Normalized phase velocity versus normalized frequency of model 1-a. The propagation angle was 45° (oblique propagation). This figure included the results performed with different time-step sizes.

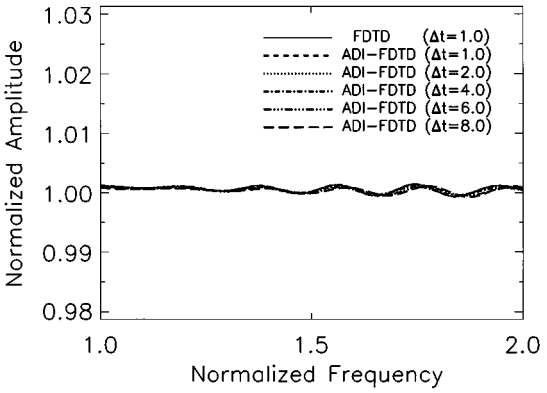

Fig. 5. Normalized amplitude versus normalized frequency of model 1-a. The propagation angle was 90° (propagated along the y-axis). This figure included the results performed with different time-step sizes.

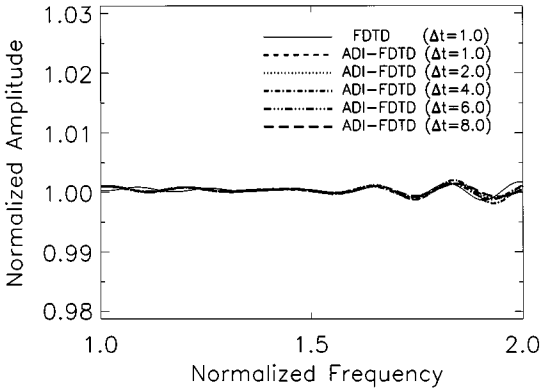

Fig. 6. Normalized amplitude versus normalized frequency of model 1-a. The propagation angle was 45° (oblique propagation). This figure included the results performed with different time-step sizes.

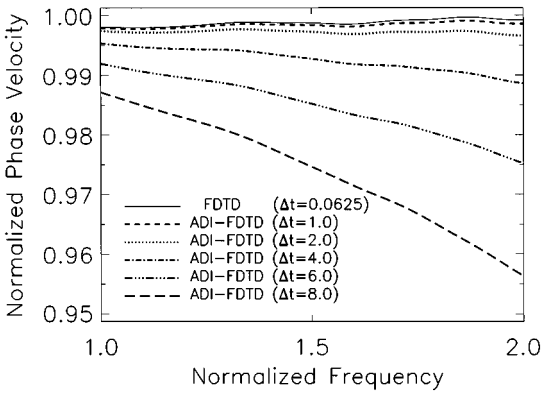

Fig. 7. Normalized phase velocity versus normalized frequency of model 1-b. The propagation angle was 90° (propagated along the y-axis). This figure included the results performed with different time-step sizes.

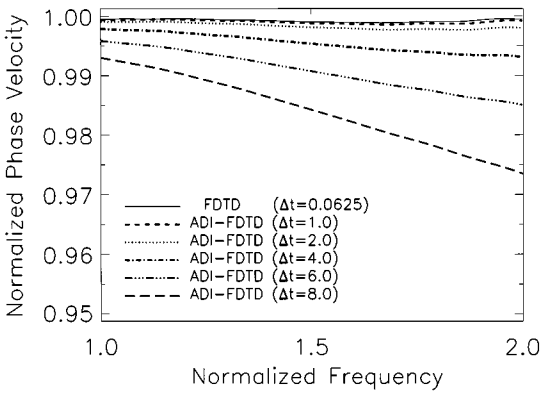

Fig. 8. Normalized phase velocity versus normalized frequency of model 1-b. The propagation angle was 45° (oblique propagation). This figure included the results performed with different time-step sizes.

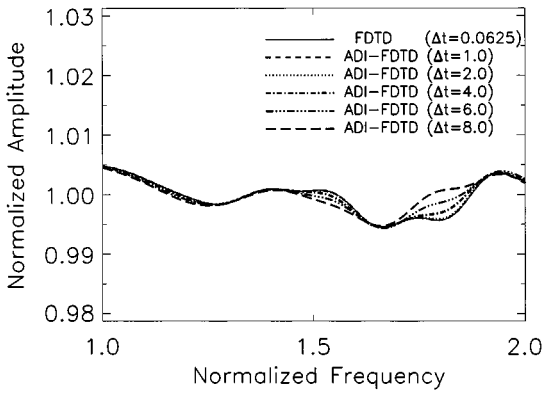

Fig. 9. Normalized amplitude versus normalized frequency of model 1-b. The propagation angle was 90° (propagated along the y-axis). This figure included the results performed with different time-step sizes.

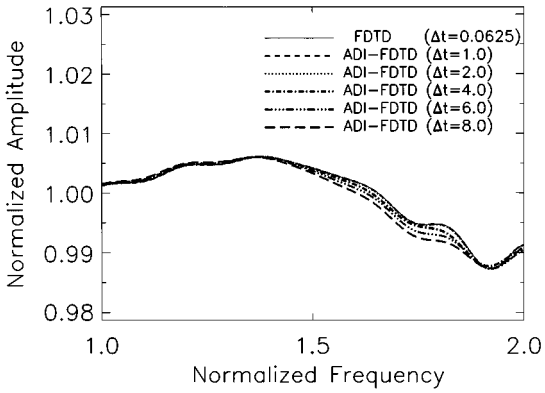

Fig. 10. Normalized amplitude versus normalized frequency of model 1-b. The propagation angle was 45° (oblique propagation). This figure included the results performed with different time-step sizes.

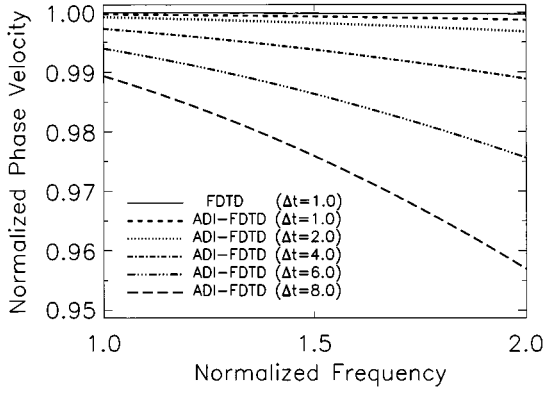

Fig. 11. Normalized phase velocity versus normalized frequency of model 2-a. This figure included the results performed with different time-step sizes.

Figs. 5 and 6 show normalized amplitudes versus the normalized frequency. Compared with phase velocity, the amplitude was independent of both the frequency and time-step size. Moreover, the error of the amplitude was much less than 1% in both cases.

⟨*Model 1-b*⟩*:* Figs. 7 and 8 show the normalized phase velocity versus the normalized frequency for different propagation angles. These results were quite similar to those of model 1-a, except that the time-step size of the conventional FDTD was much smaller. Figs. 9 and 10 show the normalized amplitudes versus the normalized frequency. The amplitude was not dependent on the time-step size, but was slightly dependent on the frequency. Compared with the results of model 1-a, the error of the amplitude was larger, but was almost less than 1%.

⟨*Model 2-a*⟩*:* Fig. 11 shows the normalized phase velocity versus the normalized frequency. Fig. 12 shows the normalized amplitude versus the normalized frequency. These results were quite similar to those of models 1-a and 1-b for a propagation angle of 90°.

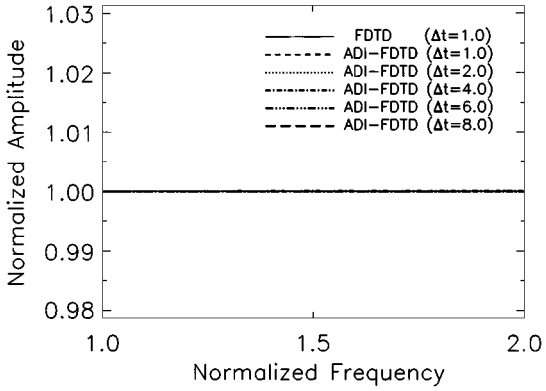

Fig. 12. Normalized amplitude versus normalized frequency of model 2-a. This figure included the results performed with different time-step sizes.

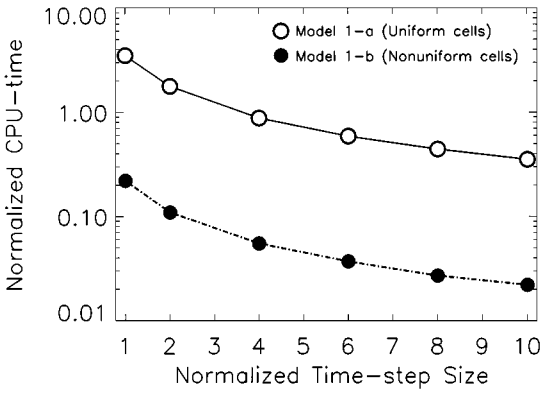

Fig. 13. Normalized CPU time versus normalized time-step size of models 1-a and 1-b.

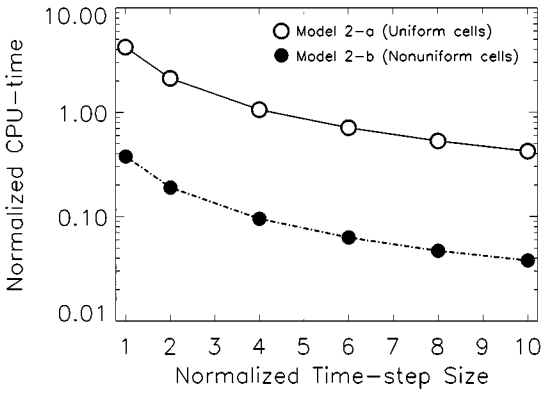

Fig. 14. Normalized CPU time versus normalized time-step size of models 2-a and 2-b.

⟨*Model 2-b*⟩*:* The results were identical to those of model 2-a, except that the time-step size in the conventional FDTD was much smaller, thus, the results were not presented.

Fig. 13 shows the required CPU time for the ADI–FDTD calculation of models 1-a and 1-b normalized by that for the conventional FDTD calculation of each model. Fig. 14 shows the required CPU time for the ADI–FDTD calculation of models 2-a and 2-b normalized by that for the conventional FDTD calculation of each model.

V. Discussion

In using uniform cells, an increase in the time-step size did not result in an amplitude error (see Figs. 5, 6, and 12), but resulted in numerical dispersion (see Figs. 3, 4, and 11). Thus, even if we use the ADI–FDTD, we cannot set a larger time-step size than the CFL limit without a decrease in phase velocity. In other words, the tradeoff of an increase in time-step size is a decrease in phase accuracy. However, there may be a problem in that the required accuracy will not be very high. For example, if the normalized frequency is 1.0 (and may be lower) and the permissible limit of numerical dispersion is 1.0%, the normalized time-step size can be set to 6.0, which is six times as large as the CFL limit (see Figs. 3, 4, and 11). The CPU time can then be reduced to about 60%–70% of the conventional FDTD, although the two methods do not achieve the same phase accuracy (see Figs. 13 and 14). This indicates that the ADI–FDTD method has the advantage of ensuring a more efficient calculation at relatively low frequencies.

In using local nonuniform cells, an increase in the time-step size also did not result in an amplitude error, though using just nonuniform cells caused an amplitude error, which was almost less than 1%, and that of the ADI–FDTD was almost the same as the conventional FDTD (see Figs. 9 and 10). The increase in the time-step size resulted in numerical dispersion (see Figs. 7 and 8). However, it is possible to set a larger time-step size than the CFL limit of the conventional FDTD without experiencing a decrease in phase accuracy. If the normalized time-step size is set to 1.0, which is 11–16 times as large as the CFL limit, the CPU time can be made about 20%–40% lower than when using the conventional FDTD while maintaining a similar level of accuracy in the two methods. If the normalized frequency is 1.0 (and may be lower) and the permissible limit of numerical dispersion is 1.0%, the normalized time-step size can be set to 6.0 and the CPU time can be reduced to about 4%–7% than that of the conventional FDTD, although the two methods do not achieve the same phase accuracy (see Figs. 13 and 14).

VI. Conclusion

This paper has presented a quantitative study on the selection of the time-step size in the ADI–FDTD method for 2-D TM and TE waves in terms of numerical error. An increase in the time-step size did not result in an amplitude error, but resulted in numerical dispersion. In using uniform cells for dividing the computational domain, we cannot set a larger time-step size than the CFL limit without experiencing a decrease in phase velocity. On the other hand, in using local nonuniform cells that includes relatively very small cells, the local minimum cell reduced the time-step size because of the CFL condition when the conventional FDTD was used. Consequently, we could set a larger time-step size when the ADI–FDTD was used without experiencing a decrease in phase accuracy. In that case, we could reduce the CPU time by using the ADI–FDTD method rather than the conventional FDTD method, and we could achieve the same level of accuracy.

REFERENCES

[1] T. Namiki, "A new FDTD algorithm based on alternating-direction implicit method," *IEEE Trans. Microwave Theory Tech.*, vol. 47, pp. 2003–2007, Oct. 1999.

[2] G. D. Smith, *Numerical Solution of Partial Differential Equations*. Oxford, U.K: Oxford Univ. Press, 1965.

[3] K. S. Yee, "Numerical solution of initial boundary value problems involving Maxwell's equations in isotropic media," *IEEE Trans. Antennas and Propagation*, vol. 14, pp. 302–307, May 1966.

[4] X. Zhang, J. Fang, and K. K. Mei, "Calculations of the dispersive characteristics of microstrips by the time-domain finite difference method," *IEEE Trans. Microwave Theory Tech.*, vol. 36, pp. 263–267, Feb. 1988.

Takefumi Namiki (M'99) was born in Chiba, Japan, in 1963. He received the B.S. degree in physics from the Tohoku University, Sendai, Japan, in 1985, and is currently working toward the Ph.D. degree at the Chiba University, Chiba, Japan.

From 1986 to 1991, he was with Fujitsu Laboratories Ltd., Atsugi, Japan, where he was engaged in research of high-speed optical modulator for optical communications systems. In 1991, he joined Fujitsu Ltd., Tokyo, Japan, where he was engaged in research and development of the computational science, and since 1994, has been engaged in research of computational electromagnetics. His research interests include numerical techniques for modeling electromagnetic fields and waves, and computer-aided engineering (CAE) systems of microwave circuits, antennas, and optical waveguides.

Mr. Namiki is a member of the Institute of Electrical, Information and Communication Engineers (IEICE), Japan.

Koichi Ito (M'81) was born in Nagoya, Japan, on June 4, 1950. He received the B.S. and M.S. degrees from Chiba University, Chiba, Japan, in 1974 and 1976, respectively, and the D.E. degree from the Tokyo Institute of Technology, Tokyo, Japan, in 1985, all in electrical engineering.

From 1976 to 1979, he was a Research Associate at the Tokyo Institute of Technology. From 1979 to 1989, he was a Research Associate at Chiba University. From 1989 to 1997, he was an Associate Professor in the Department of Electrical and Electronics Engineering, Chiba University. He is currently a Professor in the Department of Urban Environment Systems, Chiba University. In 1989, 1994, and 1998, he was an Invited Professor with Universite de Rennes I, Rennes, France. His main interests include analysis and design of printed antennas and small antennas, research on evaluation of the interaction between electromagnetic fields and the human body, and antennas for medical applications of microwaves.

Dr. Ito is a member of the American Association for the Advancement of Science (AAAS), the Institute of Electrical, Information and Communication Engineers (IEICE), Japan, the Institute of Image Information and Television Engineers of Japan, and the Japanese Society of Hyperthermic Oncology.